Front. Mater. Sci. 2019, 13(1): 33–42
https://doi.org/10.1007/s11706-019-0449-0

RESEARCH ARTICLE

Alkylamine-mediated synthesis and photocatalytic properties of ZnO

Cuicui HU[1], Huanhuan ZHANG[2], and Yanjun XING (✉)[1]

1 Key Laboratory of Science and Technology of Eco-Textiles (Ministry of Education), College of Chemistry, Chemical Engineering and Biotechnology, Donghua University, Shanghai 201620, China
2 Shanghai Institute of Quality Inspection and Technical Research, Shanghai 200233, China

ABSTRACT: A simple approach to synthesize ZnO microstructures was reported using dodecylamine, hexadecylamine and oleylamine as template agents. The synthesized ZnO was characterized by XRD, FESEM, TEM, EDS mapping, FTIR, UV–vis DRS, Raman spectroscopy and BET analysis. Hierarchical oriented ZnO microstructures were obtained. The photocatalytic performance of ZnO prepared with different types of alkylamines was evaluated by the degradation of methylene blue (MB) and methyl orange (MO). The results suggested that alkylamine control the nucleation, growth and morphology of ZnO. The photocatalytic properties of ZnO on the degradation of MB and MO decreased with increasing the alkyl chain length in alkylamine.

KEYWORDS: ZnO; controlled preparation; alkylamine; photocatalytic property

Contents

Received October 25, 2018; accepted December 3, 2018

E-mail: yjxing@mail.dhu.edu.cn

1 Introduction

Metal oxide nanostructures have attracted much attention due to their outstanding physical and chemical properties dependent on the shape and size. Among them, ZnO is a very important direct band-gap semiconductor with high band gap (3.37 eV) and exciton binding energy (60 meV) at the normal room temperature. Due to its excellent properties, it has been widely used in light-emitting materials [1], photodetectors [2], gas sensors [3], solar cells [4], piezoelectric generators [5], and antibacterials [6]. Besides, ZnO has also been used as the photocatalyst because of its high electron mobility, diversified morphology, low cost, high chemical stability [7], and environmental friendliness [8–9]. Therefore the controlled preparation of ZnO nanostructures has attracted significant interest owing to

meeting the need.

Different ZnO nanostructures have been synthesized by an amine-mediated reaction in an organic solvent [10–11], and the influence of alkylamine acting as a versatile reagent for the synthesis of various nanoparticle systems has been investigated [12–13].

We also reported the controlled preparation of different ZnO microstructures by tuning the amount of oleylamine (OLA) [14]. On that basis, further research on the influence of alkylamine (dodecylamine (DDA), hexadecylamine (HDA) and OLA) with different chain lengths on the size, morphology and structure of ZnO was studied. In this work, the role of alkylamine in the synthesis of ZnO microstructures at low temperature was investigated. The controlled formation mechanism of the hierarchical ZnO microstructure was proposed. The influence of the ZnO microstructure morphology on photocatalytic activities was also investigated by the decolorization of methylene blue (MB) and methyl orange (MO) aqueous solutions under the ultraviolet (UV) light.

2 Experimental

2.1 Materials

Materials in the experiment include zinc acetate dehydrate ($Zn(CH_3COO)_2 \cdot 2H_2O$, Sinopharm Chemical Reagent Co., Ltd.), DDA (Adamas, ⩾98%), HDA (Adamas, 90%), OLA (Adamas, ⩾90%), N,N'-dimethylformamide (DMF, Shanghai Lingfeng Chemical Reagent Co., Ltd., ⩾99.5%), absolute ethanol (Changshu Yang Yuan Chemical Co., Ltd., ⩾99.5%), commercial ZnO (Sinopharm Chemical Reagent Co., Ltd.), MB (Shanghai Reagent Factory), and MO (Sinopharm Chemical Reagent Co., Ltd.). All the chemicals used were of analytical grade and used without further purification.

2.2 Synthesis of ZnO microstructures

10 mmol DDA was added into 60 mL DMF/H_2O (v/v = 1:2), and then the mixture was stirred continuously for 30 min. Afterwards 2 mmol $Zn(CH_3COO)_2$ was further dissolved. The mixture was then heated to 85 °C, kept for 30 min, and cooled down to room temperature naturally. After centrifugation, the white precipitate was washed respectively with absolute ethanol and distilled water for several times, and freeze-dried. Under above similar conditions, the ZnO sample was prepared using HDA or OLA as the template. ZnO samples prepared under the presence of DDA, HDA and OLA were referred as ZnO-D, ZnO-H and ZnO-O, respectively.

2.3 Characterization

X-ray diffraction (XRD) patterns were obtained using a D/max 2550 V diffractometer (Rigaku, Tokyo, Japan) with Cu Kα radiation (λ = 1.5406 Å; scanning speed: 0.02(°)/s). The morphology and size of the products was characterized by field-emission scanning electron microscopy (FESEM, HITACHI S-4800, Japan) and high-resolution transmission electron microscopy (HRTEM, JEM-2100F, Japan) at an accelerating voltage of 200 kV, respectively. The energy dispersive spectroscopy (EDS) mapping (JEM-2100F, Japan) was used to analyze images of the surface topography and the location of each element. Fourier transform infrared spectroscopy (FTIR) results were recorded using PerkinElmer Spectrum Two™ FTIR spectrophotometer in the range of 4000–400 cm^{-1}. Ultraviolet–visible diffuse reflectance spectroscopy (UV–vis DRS) results of the samples were obtained in the wavelength range from 200 to 800 nm by using a Shimadzu UV3600 UV–vis spectrophotometer. Raman spectra were measured by an excitation wavelength of 532 nm (Renishaw inVia-Reflex) at room temperature. The Brunauer–Emmett–Teller (BET) surface areas of ZnO microstructures were analyzed by nitrogen adsorption/desorption isotherm determined at the liquid nitrogen temperature on a surface area and porosimetry analyzer (V-Sorb 2800P).

2.4 Photocatalytic activity measurements

The photocatalytic experiments were carried out in a BL-GHX-V photochemical reaction apparatus (Shanghai Bilon Instrument Co., Ltd.). 20 mg of prepared ZnO was dispersed into 50 mL 2.0×10^{-5} $mol \cdot L^{-1}$ MB (or MO) aqueous solution without adjusting the pH, and then mechanically stirred in the dark for 30 min to achieve adsorption/desorption equilibrium between the catalyst and the dye. The mixture was further exposed to a 360 W high-pressure mercury lamp. The system temperature was maintained at 25 °C by circulation of cold water through an external heat exchanger. At given time intervals, one of the samples was taken out and centrifuged to remove the catalysts for analysis. The concentration of MB (or MO) was determined using a PerkinElmer Lambda 35 UV–vis spectrophotometer at the maximum absorbance of 664 nm

(or 463 nm). The decolorization efficiency (η) of the dye was calculated by the equation as follow:

$$\eta/\% = \frac{c_0 - c_t}{c_0} \times 100 \quad (1)$$

where c_0 is the initial concentration of dye and c_t is the concentration of dye at time t.

3 Results and discussion

3.1 Morphology and crystal structure

XRD patterns of ZnO samples synthesized with different types of alkylamine were shown in Fig. 1. All of the observed diffraction peaks in the XRD patterns were well indexed to the (1 0 0), (0 0 2), (1 0 1), (1 0 2), (1 1 0), (1 0 3), (2 0 0), (1 1 2) and (2 0 1) planes of the hexagonal wurtzite ZnO (JCPDS card no. 36-1451) [14–15], and no other diffraction peaks of impurities were found. The results showed that the samples were single ZnO with high crystallinity. With increasing the alkylamine chain length, the crystallite sizes of ZnO-D, ZnO-H and ZnO-O calculated by the Scherrer formula according to the (1 1 0) plane were 15.52, 23.35 and 27.66 nm, respectively.

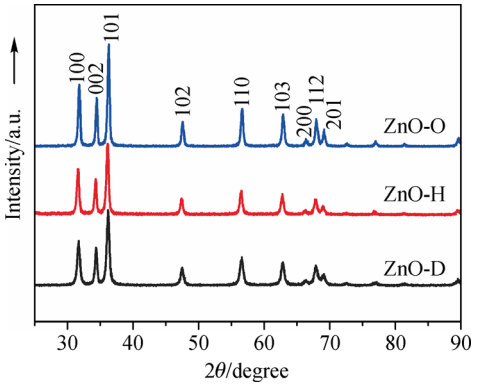

Fig. 1 XRD patterns of ZnO samples.

The corresponding SEM images were shown in Fig. 2. In Fig. 2(a), the morphology of sample ZnO-D was irregular. The average axial length was about 640 nm, and the average diameter was about 290 nm. For sample ZnO-H, the average axial length was about 860 nm, and the average diameter was about 350 nm (Fig. 2(b)). For sample ZnO-O, the uniform brush-like structure was obtained. The total axial length was about 1–2 μm. The handle part of ZnO-O was with the average length of 560 nm and the diameter of about 300 nm. The width of pyramidal end of ZnO-O was in the range of about 400–900 nm (Fig. 2(c)) [14]. It revealed that the ZnO samples prepared had the hierarchical structure. The orientation growth of the ZnO samples along the *c*-axis direction was more obvious with the increase of the alkyl chain length in alkylamine. Moreover, the size of prepared ZnO samples increased with the length increase of the alkylamine chain. This result was consistent with the XRD calculations.

The morphologies of ZnO microstructures prepared using DDA and HDA were characterized by TEM. The corresponding TEM images are shown in Fig. 3. It can be seen that ZnO-D and ZnO-H were of the hierarchical columnar structures (Figs. 3(a) and 3(d)). The diffraction rings in the SAED pattern indicated that ZnO samples were in crystalline forms (Figs. 3(b) and 3(e)) [16]. The HRTEM image of ZnO-D in Fig. 3(c) revealed a lattice spacing of 0.26 nm, which corresponded well to the *d* spacing of the (0 0 2) plane of hexagonal ZnO. For sample ZnO-H, the lattice spacing of 0.52 nm was observed (Fig. 3(f)), which corresponded to the *d* spacing of the (0 0 1) plane. Moreover, according to the TEM image of ZnO-O [14], these ZnO samples mainly grew in the [0 0 0 1] direction.

The corresponding EDS mapping images of samples ZnO-D and ZnO-O were shown in Fig. 4. A homogeneous distribution of elements Zn and O in samples ZnO-D and ZnO-O could be observed. It also exhibited trace amounts of C and N, which ubiquitously distributed over the same area (Figs. 4(d), 4(e), 4(i) and 4(j)). The C and N signals

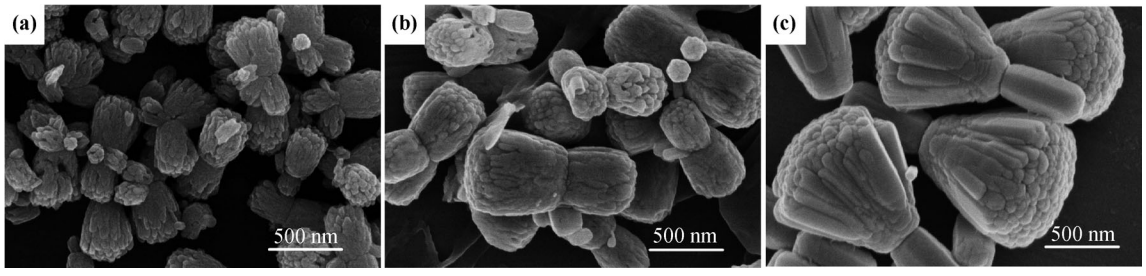

Fig. 2 FESEM images of ZnO samples: **(a)** ZnO-D; **(b)** ZnO-H; **(c)** ZnO-O [14].

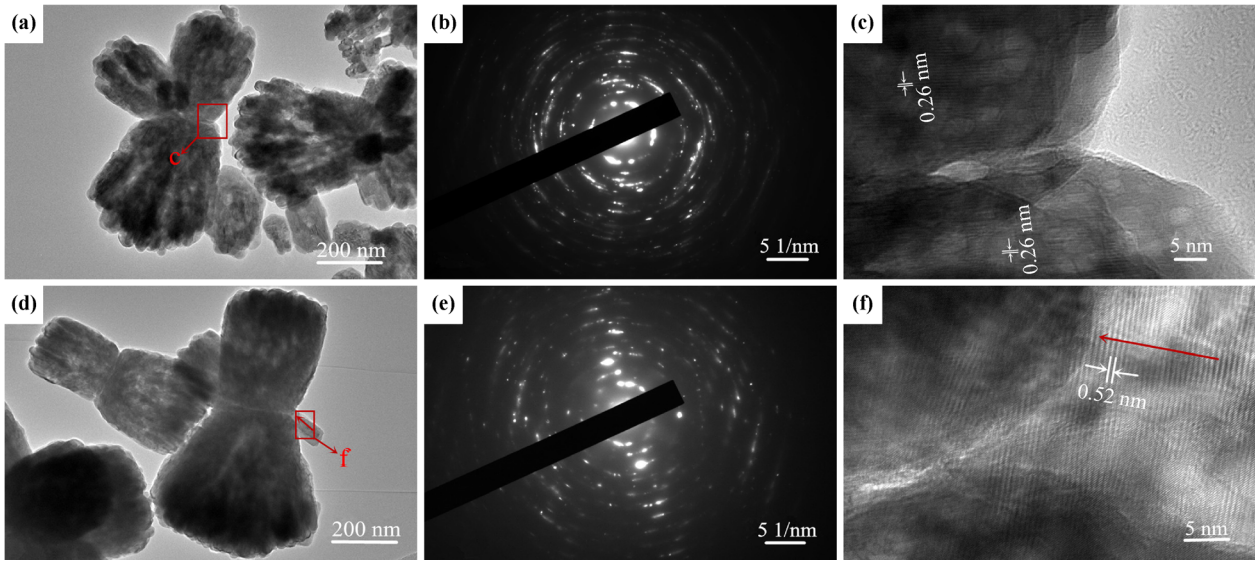

Fig. 3 **(a)(d)** TEM images, **(b)(e)** SAED patterns and **(c)(f)** HRTEM images of samples ZnO-D (upper) and ZnO-H (lower).

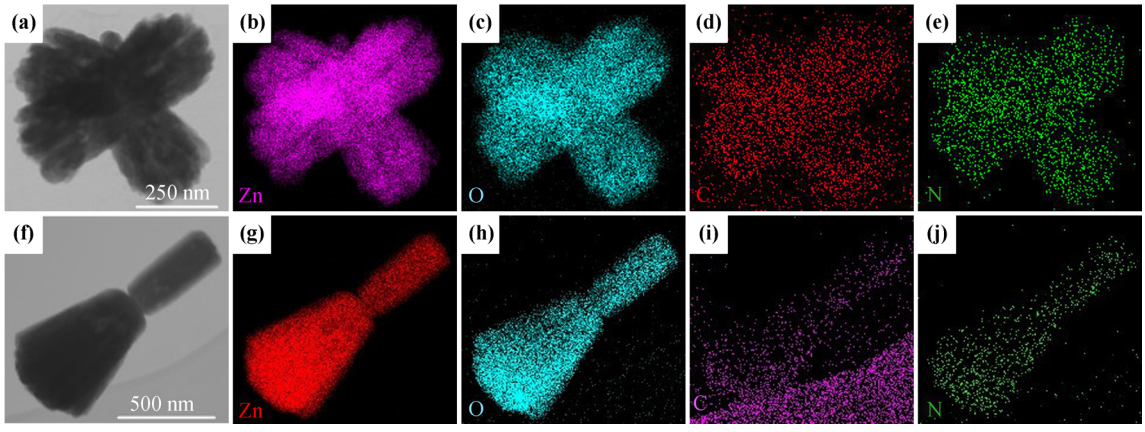

Fig. 4 EDS mapping images of **(a)(b)(c)(d)(e)** sample ZnO-D and **(f)(g)(h)(i)(j)** sample ZnO-O.

indicated the presence of DDA and OLA in samples ZnO-D and ZnO-O, implying that the formation and growth of the ZnO sample was controlled by alkylamine.

FTIR spectra of ZnO samples were revealed in Fig. 5. It can be seen that the strong peak around 400–600 cm^{-1} was attributed to a distinct stretching mode of crystal ZnO. The broad absorption band at 3050–3650 cm^{-1} was due to the O–H stretching of water molecules adsorbed on the surface of ZnO. The peaks at 2849 and 2910 cm^{-1} were assigned to the C–H stretching modes of the alkylamine carbon chain [17]. Compared with commercial ZnO, it suggested that there was alkylamine adsorbed on the surfaces of ZnO samples. The bands in the region of 1700–1000 cm^{-1} corresponded to C = O (in CH_3COO^-), C–N (in amine) and C–H vibrations, respectively [18]. Therefore, it was concluded that alkylamine as the template agent adsorbed on the surface of ZnO controlled the growth and morphology of ZnO.

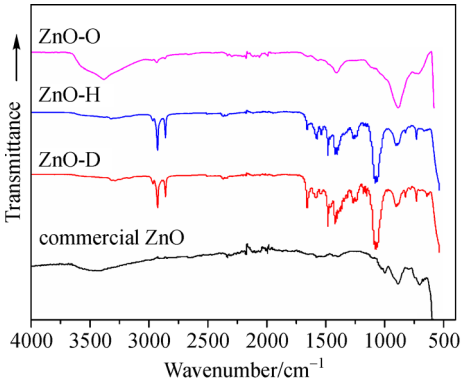

Fig. 5 FTIR spectra of ZnO samples.

3.2 The growth mechanism

According to above experimental results, the schematic diagram of the formation process of ZnO samples was illustrated in Fig. 6. A self-assembled hexagonal lamella of ZnO nuclei was formed in the initial crystal growth stage. As a template agent, the non-polar long carbon chain of alkylamine was more likely to be adsorbed on the non-polar surfaces of ZnO. The polar facets were exposed and the ZnO crystal grew in the [0 0 0 1] direction to the columnar structure [19]. A complex was formed between Zn^{2+} and alkylamine firstly. The hydrolysis ability of this complex depended on the length of the alkylamine carbon chain. Compared with DDA and HDA, OLA showed lower hydrolysis ability and higher stability. As a result, ZnO-O was easy to form an oriented growth during the reaction. Moreover, with the increase of the carbon chain in amines, the binding of non-polar long carbon chain to the non-polar surface of ZnO increased, which also promoted the orientation growth of the ZnO structure. Due to the shorter length of the DDA carbon chain, the complex between Zn^{2+} and DDA formed in water had high hydrolysis ability and poor stability. As a result, ZnO-D showed a disorganized morphology [20]. The result indicated that the particle size and the distribution were also controlled by the alkyl chain length. Therefore, different alkylamine types and chain lengths can effectively control the growth process and further regulate the size and morphology of ZnO microstructures.

3.3 Optical property

UV–vis DRS results of ZnO samples were presented in Fig. 7(a). All the ZnO samples showed strong absorption in the UV region. Their absorption edges were about 387 nm (ZnO-D), 392 nm (ZnO-H) and 394 nm (ZnO-O), respectively. The band gap (E_g) values of ZnO-D, ZnO-H and ZnO-O were 3.21, 3.17 and 3.16 eV, respectively, which were determined by extrapolating the linear part of the plots of $(\alpha hv)^2$ versus the energy of absorbed light (Fig. 7(b)) [21]. The results indicated that ZnO-O was easier to obtain energy to generate electron–hole pairs, which was beneficial to increase the photocatalytic activity. However, the oxidation ability of photogenerated electron–hole pair of column-like ZnO-D would be stronger than that of brush-like ZnO-O, which was also conducive to improve the photocatalytic efficiency.

Figure 8 showed Raman spectra of ZnO samples. The strongest peak at 437–440 cm^{-1} was attributed to the E_2^{high} mode. It suggested that the prepared ZnO samples were in the typical wurtzite structure and had high crystalline quality [22–23], which was consistent with the XRD results. The peak at 578–581 cm^{-1} was attributed to the LO mode, caused by the defects in the sample [24]. In addition, the intensity ratio between the E_2^{high} mode and the LO mode can be clearly seen in Table 1. The $I(E_2^{high})/I(LO)$ values indicated that ZnO-O had higher crystalline quality among the three ZnO samples [23,25].

3.4 BET surface area analysis

To investigate the specific areas and the porous nature of ZnO samples, BET gas sorption measurement was performed. The nitrogen desorption/adsorption isotherms and corresponding Barret–Joyner–Halenda (BJH) pore size

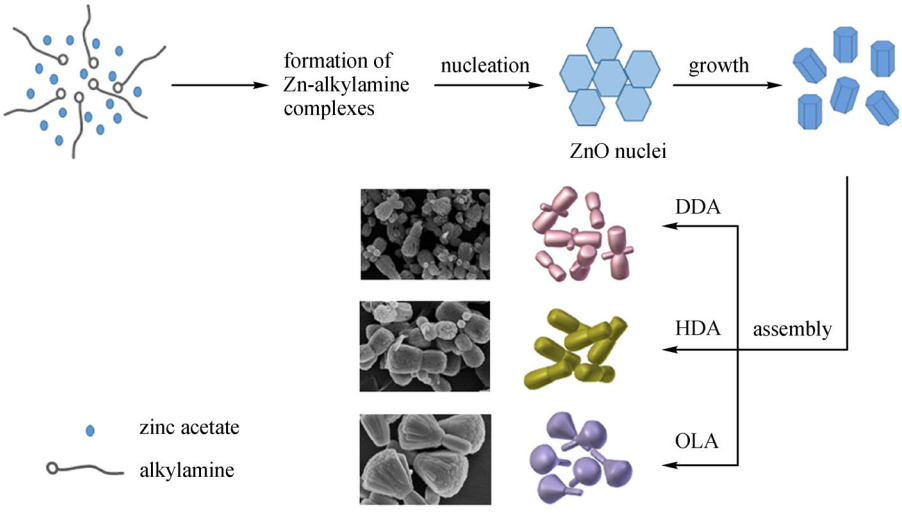

Fig. 6 Schematic illustration of the formation process of ZnO samples.

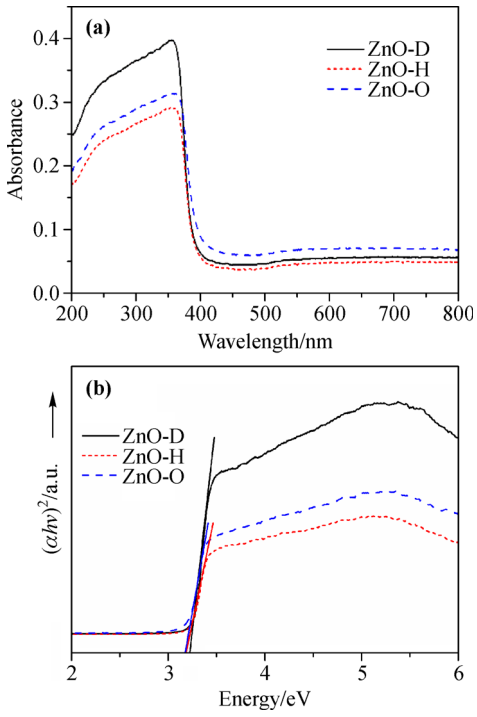

Fig. 7 **(a)** UV–vis DRS results and **(b)** plots of $(\alpha h\nu)^2$ versus the energy of absorbed light of ZnO samples.

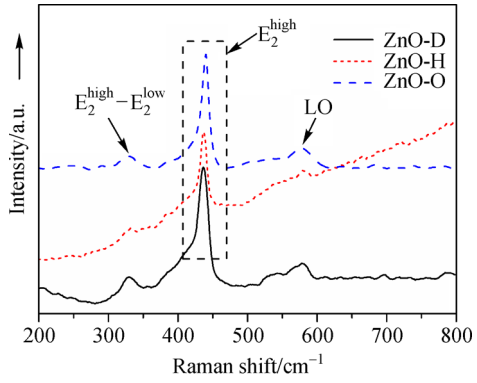

Fig. 8 Raman spectra of ZnO samples.

Table 1 Intensity ratios between E_2^{high} mode and LO mode

Sample	$I(E_2^{high})/I(LO)$
ZnO-D	1.27
ZnO-H	1.09
ZnO-O	5.29

distribution curves of ZnO samples were shown in Fig. 9. All the samples displayed the type IV isotherms and type H3 hysteresis loops, which confirmed the characteristic mesoporous nature of ZnO samples, according to the IUPAC classification [26]. In addition, the surface area, pore volume, and pore size of ZnO samples were presented

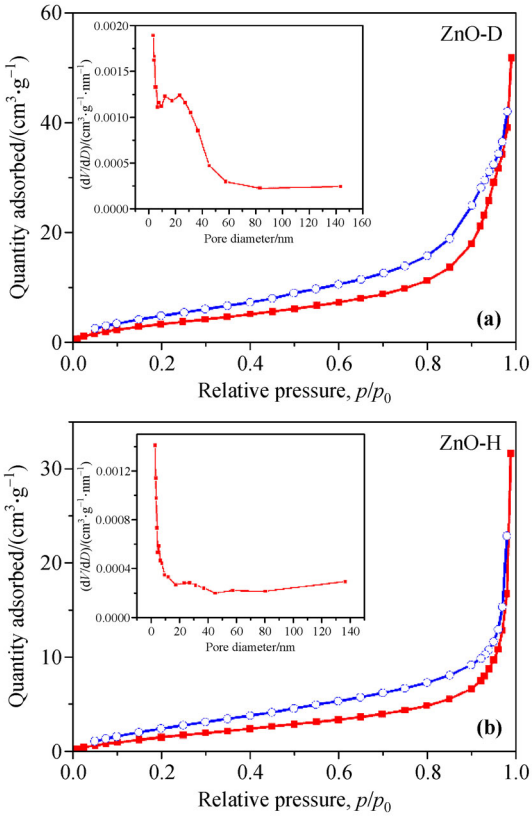

Fig. 9 Nitrogen adsorption/desorption isotherms of ZnO samples: **(a)** ZnO-D; **(b)** ZnO-H. Inset: the corresponding BJH pore size distribution.

in Table 2. It can be seen that the order of the BET surface area from big to small is S_{BET}(ZnO-O) > S_{BET}(ZnO-D) > S_{BET}(ZnO-H).

Table 2 Values of S_{BET}, pore volume and pore size of ZnO samples

Sample	S_{BET}[a)]/(m^2·g^{-1})	Pore volume[b)]/(cm^3·g^{-1})	Pore size[c)]/nm
ZnO-D	14.87	0.08	3.42
ZnO-H	7.11	0.05	3.06
ZnO-O [14]	15.48	0.02	12.38

a) The BET surface area is calculated from the linear part of the BET plot (p/p_0 = 0.05–0.3).
b) Pore volume is determined by adsorption branch of the nitrogen isotherms at p/p_0 = 0.990.
c) Average pore size is estimated using the adsorption branch of nitrogen isotherms and the BJH method.

3.5 Photocatalytic activities

Figure 10 showed the photocatalytic degradation of the MB solution in the presence of different ZnO samples. The changes of UV–vis absorption spectra of the MB aqueous solution in the presence of different ZnO samples were depicted in Figs. 10(a)–10(c). It was observed that the absorption of MB at 664 nm decreased with the increase of

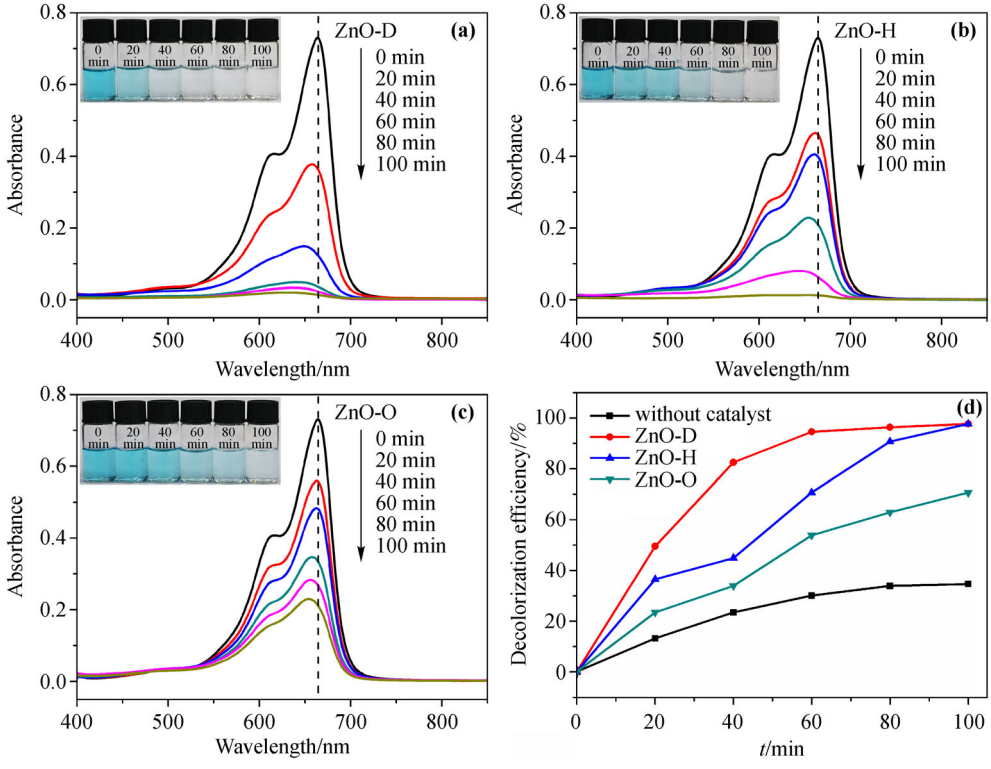

Fig. 10 **(a)(b)(c)** UV–vis absorption spectra and corresponding photographs (inset) of MB solutions during the photocatalytic reaction in the presence of ZnO-D, ZnO-H and ZnO-O. **(d)** Decolorization efficiency of the MB solution.

the reaction time. For samples ZnO-D and ZnO-H, the main absorption peak of MB almost disappeared after 100 min. No new absorption peak was observed in the UV–vis region. This indicated that the photocatalytic degradations of MB using ZnO-D and ZnO-H as photocatalysts were complete (inset photographs). For ZnO-O, the absorption of MB at 664 nm decreased slowly under the UV irradiation. The photocatalytic degradation of MB was incomplete after 100 min. The maximum absorption wavelength of MB displayed a blue shift gradually after the irradiation, which suggested that the chromophore in MB was incompletely decomposed [27]. The dependencies of decolorization efficiency on irradiation time for all the samples were presented in Fig. 10(d). The preliminary experiment showed that MB can be slightly degraded under the UV light irradiation without ZnO samples. The final decolorization efficiencies of MB were 97.5%, 97.4% and 70.5% for ZnO-D, ZnO-H and ZnO-O, respectively.

Figure 11 showed the photocatalytic degradation of the MO solution in the presence of different ZnO samples. The changes of UV–vis absorption spectra of the MO aqueous solution in the presence of different ZnO samples were similar to MB (Figs. 11(a)–11(c)). For ZnO-D and ZnO-H as photocatalysts, the photocatalytic degradations of MO were almost complete. For ZnO-O, the photocatalytic degradation of MO was incomplete after 100 min. The maximum absorption wavelength of MO also displayed a blue shift gradually after the irradiation [28]. The final decolorization efficiencies of MO (Fig. 11(d)) were 90.8% (ZnO-D), 86.9% (ZnO-H) and 59.6% (ZnO-O), respectively. In addition, ZnO-O had the highest degradation efficiency on the degradation of MO in the initial 20 min reaction (Fig. 11(d)), which may be due to the large specific surface area and the resulted high adsorption capacity of ZnO-O.

From the above experiments, it can be seen that the photocatalytic performances of ZnO-D and ZnO-H were relatively higher for MB or MO. This might be due to the smaller size and morphology, the lower orientations, the more polar planes and the defects of samples ZnO-D and ZnO-H [29]. As compared to the size effect, the morphologic effect on photocatalytic activity of ZnO samples was more dominant [30]. The decrease of the length of the carbon chain in alkylamine (as template) would lead to an increased exposure of the polar (0 0 1) face of ZnO [14,30]. The exposure of the polar (0 0 1) face could positively enhance the surface oxygen vacancy content in ZnO [29] and accelerate the production of •OH

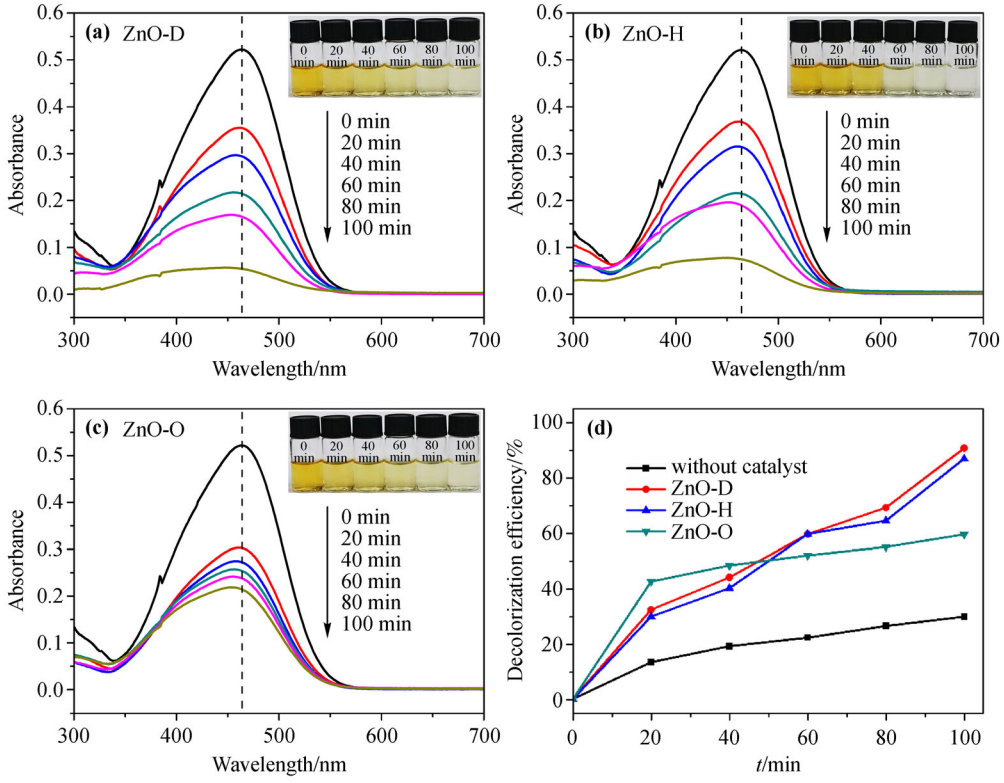

Fig. 11 **(a)(b)(c)** UV–vis absorption spectra and corresponding photographs (inset) of MO solutions during photocatalytic reaction in the presence of ZnO-D, ZnO-H and ZnO-O [14]. **(d)** Decolorization efficiency of the MO solution.

radicals on the surface of ZnO [30], both of which were beneficial for the photocatalytic degradation of dyes. As a result, the photocatalytic activity increased with decreasing the alkyl chain length in alkylamine. Moreover, the C or N doping in the prepared ZnO samples, especially in ZnO-D, also enhanced the photocatalytic activity [31–32]. In addition, the decolorization effect of the prepared ZnO samples on the MB solution was better than that of the MO solution, which may be related to the structure and properties of the dye itself [16].

A comparison of the photocatalytic degradation performance of reported ZnO catalysts and as-synthesized ZnO-D had been summarized in Table 3 [33–38]. It demonstrated that ZnO-D showed comparable photocatalytic activity to those of reported ZnO samples.

4 Conclusions

In summary, a simple and facile approach to achieve shape-controlled ZnO microstructures using alkylamine under the condition of low temperature and open system was reported in this work. The results suggested that alkylamine control the nucleation, growth and morphology of ZnO

Table 3 Comparison between the reported catalysts and the current catalysts [33–38]

Sample	Light source	Experimental conditions	Photodegradation efficiency	Ref.
ZnO	250 W, mercury lamp	c(catalyst) = 1 g/L, c(MB) = 1.7×10^{-4} mol/L	96.2% after 70 min	[33]
ZnO	UV light	c(catalyst) = 1 g/L, c(MB) = 3×10^{-5} mol/L	97% after 120 min	[34]
ZnO	UV radiation	c(catalyst) = 1 g/L, c(MB) = 1×10^{-5} mol/L, pH = 7	97.54% after 240 min	[35]
ZnO	360 W, mercury lamp	c(catalyst) = 0.4 g/L, c(MO) = 2×10^{-5} mol/L	97.1% after 100 min	[36]
ZnO	300 W, mercury lamp	c(catalyst) = 0.4 g/L, c(MO) = 50 mg/L	50% after 120 min	[37]
ZnO	125 W, mercury lamp	c(catalyst) = 0.2 g/L, c(MO) = 20 mg/L, pH = 7	~100% after 80 min	[38]
ZnO-D	360 W, mercury lamp	c(catalyst) = 0.4 g/L, c(MB) = 2×10^{-5} mol/L	97.5% after 100 min	this work
ZnO-D	360 W, mercury lamp	c(catalyst) = 0.4 g/L, c(MO) = 2×10^{-5} mol/L	90.8% after 100 min	this work

microstructures, and photocatalytic properties of ZnO on the degradation of MB and MO decreased with increasing the alkyl chain length in alkylamine.

Disclosure of potential conflicts of interests The authors declare that they have no conflict of interest.

Acknowledgements This work was supported by the Fundamental Research Funds for the Central Universities (Grant No. 2232013A3-05) and the National Science and Technology Ministry (ID 2012BAK30B03).

References

[1] Pauporté T, Lupan O, Viana B, et al. Controlling the properties of electrodeposited ZnO nanowire arrays for light emitting diode, photodetector and gas sensor applications. In: Proceedings SPIE 8987: Oxide-based Materials and Devices V, International Society for Optics and Photonics, 2014, 89871R

[2] Farhat O, Halim M, Ahmed N M, et al. A study of the effects of aligned vertically growth time on ZnO nanorods deposited for the first time on Teflon substrate. Applied Surface Science, 2017, 426: 906–912

[3] Diao K, Zhou M, Zhang J, et al. High response to H_2S gas with facile synthesized hierarchical ZnO microstructures. Sensors and Actuators B: Chemical, 2015, 219: 30–37

[4] Canto-Aguilar E J, Rodríguez-Pérez M, García-Rodríguez R, et al. ZnO-based dye-sensitized solar cells: Effects of redox couple and dye aggregation. Electrochimica Acta, 2017, 258: 396–404

[5] Hu Y, Wang Z L. Recent progress in piezoelectric nanogenerators as a sustainable power source in self-powered systems and active sensors. Nano Energy, 2015, 14(SI): 3–14

[6] Esparza-González S C, Sánchez-Valdés S, Ramírez-Barrón S N, et al. Effects of different surface modifying agents on the cytotoxic and antimicrobial properties of ZnO nanoparticles. Toxicology In Vitro, 2016, 37: 134–141

[7] Yang P, Song X, Jia C, et al. Metal-organic framework-derived hierarchical ZnO/NiO composites: Morphology, microstructure and electrochemical performance. Journal of Industrial and Engineering Chemistry, 2018, 62: 250–257

[8] da Silva G T S T, Carvalho K T G, Lopes O F, et al. Synthesis of ZnO nanoparticles assisted by N sources and their application in the photodegradation of organic contaminants. ChemCatChem, 2017, 9(19): 3795–3804

[9] Weng Y C, Hsiao K T. Composition optimization of ZnO-based photocatalyst arrays by scanning electrochemical microscopy and the characterization of efficient photocatalysts. International Journal of Hydrogen Energy, 2015, 40(8): 3238–3248

[10] Zhang S, Chen H S, Matras-Postolek K, et al. ZnO nanoflowers with single crystal structure towards enhanced gas sensing and photocatalysis. Physical Chemistry Chemical Physics, 2015, 17 (45): 30300–30306

[11] Zhang Z, Lu M, Xu H, et al. Shape-controlled synthesis of zinc oxide: a simple method for the preparation of metal oxide nanocrystals in non-aqueous medium. Chemistry, 2007, 13(2): 632–638

[12] Mourdikoudis S, Liz-Marzán L M. Oleylamine in nanoparticle synthesis. Chemistry of Materials, 2013, 25(9): 1465–1476

[13] Mntungwa N, Khan M, Mlowe S, et al. A simple route to alkylamine capped antimony nanoparticles. Materials Letters, 2015, 145: 239–242

[14] Hu C C, Lu L, Zhu Y J, et al. Morphological controlled preparation and photocatalytic activity of zinc oxide. Materials Chemistry and Physics, 2018, 217: 182–191

[15] Patil V L, Vanalakar S A, Patil P S, et al. Fabrication of nanostructured ZnO thin films based NO_2 gas sensor via SILAR technique. Sensors and Actuators B: Chemical, 2017, 239: 1185–1193

[16] Trandafilović L V, Jovanović D J, Zhang X, et al. Enhanced photocatalytic degradation of methylene blue and methyl orange by ZnO:Eu nanoparticles. Applied Catalysis B: Environmental, 2017, 203: 740–752

[17] Rakhshanipour M, Mir N, Heidari A, et al. A simple and novel synthesis of ZnO nanohemispheres. In: 1st National Conference of Chemical and Petrochemical, 2014, 1–6

[18] Xiong H M, Shchukin D G, Möhwald H, et al. Sonochemical synthesis of highly luminescent zinc oxide nanoparticles doped with magnesium(II). Angewandte Chemie International Edition, 2009, 48(15): 2727–2731

[19] Chen Y, Peng D L, Lin D, et al. Preparation and magnetic properties of nickel nanoparticles via the thermal decomposition of nickel organometallic precursor in alkylamines. Nanotechnology, 2007, 18(50): 505703

[20] Yamamoto M, Nakamoto M. Novel preparation of monodispersed silver nanoparticles via amine adducts derived from insoluble silver myristate in tertiary alkylamine. Journal of Materials Chemistry, 2003, 13(9): 2064–2065

[21] Lv Y, Yu L, Huang H, et al. Application of the soluble salt-assisted route to scalable synthesis of ZnO nanopowder with repeated photocatalytic activity. Nanotechnology, 2012, 23(6): 065402

[22] Fukushima H, Uchida H, Funakubo H, et al. Evaluation of oxygen vacancies in ZnO single crystals and powders by micro-Raman spectroscopy. Journal of the Ceramic Society of Japan, 2017, 125 (6): 445–448

[23] Lv Y, Zhang Z, Yan J, et al. Growth mechanism and photoluminescence property of hydrothermal oriented ZnO nanostructures evolving from nanorods to nanoplates. Journal of Alloys and Compounds, 2017, 718: 161–169

[24] Russo V, Ghidelli M, Gondoni P, et al. Multi-wavelength Raman scattering of nanostructured Al-doped zinc oxide. Journal of Applied Physics, 2014, 115(7): 073508

[25] Chen K J, Fang T H, Hung F Y, et al. The crystallization and physical properties of Al-doped ZnO nanoparticles. Applied Surface Science, 2008, 254(18): 5791–5795

[26] Kruk M, Jaroniec M. Gas adsorption characterization of ordered organic–inorganic nanocomposite materials. Chemistry of Materials, 2001, 13(10): 3169–3183

[27] Chiu W S, Khiew P S, Cloke M, et al. Photocatalytic study of two-dimensional ZnO nanopellets in the decomposition of methylene blue. Chemical Engineering Journal, 2010, 158(2): 345–352

[28] Chen T, Zheng Y, Lin J M, et al. Study on the photocatalytic degradation of methyl orange in water using Ag/ZnO as catalyst by liquid chromatography electrospray ionization ion-trap mass spectrometry. Journal of the American Society for Mass Spectrometry, 2008, 19(7): 997–1003

[29] Li G R, Hu T, Pan G L, et al. Morphology–function relationship of ZnO: Polar planes, oxygen vacancies, and activity. The Journal of Physical Chemistry C, 2008, 112(31): 11859–11864

[30] Mclaren A, Valdes-Solis T, Li G, et al. Shape and size effects of ZnO nanocrystals on photocatalytic activity. Journal of the American Chemical Society, 2009, 131(35): 12540–12541

[31] Yu W, Zhang J, Peng T. New insight into the enhanced photocatalytic activity of N-, C- and S-doped ZnO photocatalysts. Applied Catalysis B: Environmental, 2016, 181: 220–227

[32] Byzynski G, Melo C, Volanti D P, et al. The interplay between morphology and photocatalytic activity in ZnO and N-doped ZnO crystals. Materials & Design, 2017, 120: 363–375

[33] Umar A, Chauhan M S, Chauhan S, et al. Large-scale synthesis of ZnO balls made of fluffy thin nanosheets by simple solution process: structural, optical and photocatalytic properties. Journal of Colloid and Interface Science, 2011, 363(2): 521–528

[34] Saravanan R, Thirumal E, Gupta V K, et al. The photocatalytic activity of ZnO prepared by simple thermal decomposition method at various temperatures. Journal of Molecular Liquids, 2013, 177: 394–401

[35] Phuruangrat A, Thongtem S, Thongtem T. Ultrasonic-assisted synthesis and photocatalytic performance of ZnO nanoplates and microflowers. Materials & Design, 2016, 107: 250–256

[36] Bao Y, Wang C, Ma J Z. Morphology control of ZnO microstructures by varying hexamethylenetetramine and trisodium citrate concentration and their photocatalytic activity. Materials & Design, 2016, 101: 7–15

[37] Chen C, Liu J, Liu P, et al. Investigation of photocatalytic degradation of methyl orange by using nano-sized ZnO catalysts. Advances in Chemical Engineering and Science, 2011, 1(1): 9–14

[38] Ghule L, Patil A, Sapnar K, et al. Photocatalytic degradation of methyl orange using ZnO nanorods. Environmental Toxicology and Chemistry, 2011, 93(4): 623–634